

Application of Graded Finite Elements for Asphalt Pavements

William G. Buttlar¹; Glaucio H. Paulino²; and Seong Hyeok Song³

Abstract: Asphalt paving layers, particularly the surface course, exhibit vertically graded material properties. This grading is caused primarily by temperature gradients and aging related stiffness gradients. Most conventional existing analysis models do not directly account for the continuous grading of properties in flexible pavement layers. As a result, conventional analysis methods may lead to inaccurate prediction of pavement responses and distress under traffic and environmental loading. In this paper, a theoretical formulation for the graded finite element method is provided followed by an implementation using the user material subroutine (*UMAT*) capability of the finite element software *ABAQUS*. Numerical examples using the *UMAT* are provided to illustrate the benefits of using graded elements in pavement analysis.

DOI: 10.1061/(ASCE)0733-9399(2006)132:3(240)

CE Database subject headings: Fractures; Asphalt pavements; Finite element method; Material properties.

Introduction

Modern pavement design procedures involve structural modeling of the layered pavement system, as a tool to select and optimize materials and layer thickness to satisfy the design criteria for pavement serviceability under anticipated traffic loads and environmental conditions. Ideally, the structural model used for design will accurately estimate the critical responses in the pavement system and predict, as a function of time, distress development such as fatigue, fracture, and permanent deformation. There are many complexities to consider in properly modeling flexible pavement systems, including: nonlinear material behavior, variable interface conditions, complex tire load patterns, and temperature and asphalt aging effects. Most of these complexities can be adequately addressed by using finite element modeling approaches (Myers et al. 2001; Kim and Buttlar 2002; Bozkurt and Buttlar 2002). It can be argued that the most important aspect of flexible pavement modeling is the proper treatment of near-surface materials, since this region is in direct contact with vehicular loads and environment. Proper analysis is critical

in the design of layer thickness and selection of surface materials to avoid premature failure.

One shortcoming of commercially available finite element codes at the present time is the inability to properly handle severe material property gradients within elements. In particular, oxidative hardening of the asphalt surface course is known to create a severe modulus gradient with depth (Mirza and Witzczak 1995). Of course, one benefit of the finite element method is the ability to assign different material properties to elements in the mesh and as a result, one can approximate a material property gradient by assigning different properties to successive layers in the model. In pavement, this layered approach has been quite common (Kim and Buttlar 2002; Sangpetngam et al. 2004; AASHTO 2002). The following quotation extracted from the AASHTO design guide is a good example illustrating the prevalence of the layered approach in the analysis of pavements. "The original pavement structure defined by the user usually has 4 to 6 layers. However, the Design Guide software may subdivide the pavement structure into 12 to 15 sublayers for the modeling of temperature and moisture variations. The Design Guide software performs the sublayering internally based on the material type, layer thickness and the location of the layer within the pavement structure." However, this approach requires a very fine mesh to achieve accuracy, which can lead to excessive solution times. This is particularly critical in pavements, where three dimensional modeling is generally required, due to geometric asymmetries (Kim 1999; Myers et al. 2001).

Thus, it is desirable to model the material property variation at the element level so that coarser meshes can be used, while maintaining accuracy. Recently such elements (called graded finite elements) have been developed and applied to functionally graded materials (FGMs) (Santare and Lambros 2000; Kim and Paulino 2002a). Significant advances have been made in the analysis of FGMs using graded finite elements including fracture mechanics investigations involving stress intensity factors and *T*-stress evaluation (Kim and Paulino 2002b; Kim and Paulino 2003). Unlike traditional laminated composites, in FGMs the material grading is continuous. This has the benefit of avoiding stress concentration and delamination, leading to a more durable

¹Associate Professor, Dept. of Civil and Environmental Engineering, Univ. of Illinois at Urbana-Champaign, 1212 Newmark Lab., 205 North Mathews Avenue, MC-250, Urbana, IL 61801. E-mail: buttlar@uiuc.edu

²Professor, Dept. of Civil and Environmental Engineering, Univ. of Illinois at Urbana-Champaign, 2209 Newmark Lab., 205 North Mathews Avenue, MC-250, Urbana, IL 61801 (corresponding author). E-mail: paulino@uiuc.edu

³Graduate Research Assistant, Dept. of Civil and Environmental Engineering, Univ. of Illinois at Urbana-Champaign, 2204 Newmark Lab., 205 North Mathews Avenue, MC-250, Urbana, IL 61801. E-mail: shsong@uiuc.edu

Note. Associate Editor: Arif Masud. Discussion open until August 1, 2006. Separate discussions must be submitted for individual papers. To extend the closing date by one month, a written request must be filed with the ASCE Managing Editor. The manuscript for this paper was submitted for review and possible publication on February 25, 2004; approved on June 23, 2005. This paper is part of the *Journal of Engineering Mechanics*, Vol. 132, No. 3, March 1, 2006. ©ASCE, ISSN 0733-9399/2006/3-240-249/\$25.00.

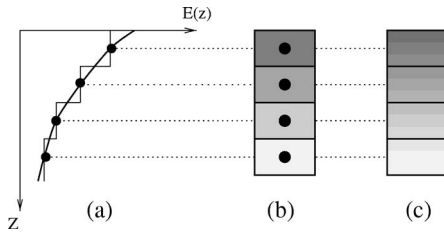


Fig. 1. Homogeneous versus graded finite elements: (a) property variation along one coordinate axis; (b) homogeneous elements; and (c) graded elements. Notice that the property of the homogeneous elements corresponds to the property at the centroids of the graded elements.

material. Although the initial emphasis in FGM development was for thermal barrier coating for spacecraft (Hirano et al. 1990), many other applications have followed. These include nuclear breeder reactors (Igari et al. 1990), high density magnetic recording media (Tani and Liu 1993), and biomaterials, such as dental and other implants (Watari et al. 1996; Oonishi et al. 1994). Although an aged asphalt pavement is graded by environmental causes rather than by design, many of the analysis tools used to analyze FGMs can be applied or modified for use in flexible pavement analysis and design. Such is the motivation for the current work.

Thus, the graded finite elements are advantageous for two main reasons: (1) to model material gradient in a single pavement layer such as the stiffening effect induced by aging of the top asphalt layer; (2) to model material gradient between two adjoining layers by means of a smooth transition of material properties (rather than a sharp transition as in the traditional approach). The graded interlayer simulates the actual merit of materials that may occur in engineering practice. The graded interlayer leads to smoother and more reliable interfacial stress.

The objectives of this paper are (1) to present the theoretical framework for graded finite elements; (2) to verify user-defined subroutine *UMAT* through which the graded elements are implemented in the finite element software *ABAQUS* (2004); and (3) to illustrate the benefits of the graded finite elements by means of numerical examples of pavement systems, which emphasize the first reason above.

Graded Finite Elements

Graded elements can be compared with conventional homogeneous elements such as those used in traditional layered analysis of pavement, as illustrated by Fig. 1. Notice that the graded element incorporates the material property gradient at the size scale of the element, while the homogeneous element produces a step-wise constant approximation to a continuous material property field such as the one shown in Fig. 1. Graded elements are implemented by means of direct sampling properties at the Gauss points of the element (Santare and Lambros 2000; Kim and Paulino 2002a), as illustrated by Fig. 2. The finite element stiffness matrix relations can be written as (Hughes 1987)

$$\mathbf{K}^e \mathbf{u}^e = \mathbf{F}^e \quad (1)$$

with

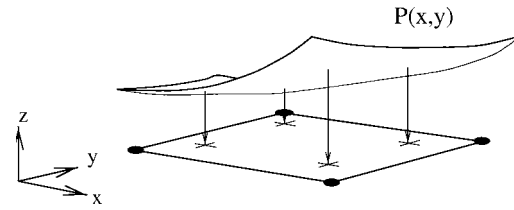


Fig. 2. Graded element with direct sampling of properties at the Gauss points. The notation $P(x,y)$ denotes a generic material property such as Young's modulus $[E(x,y)]$ and Poisson's ratio $[\nu(x,y)]$ in isotropic elasticity analysis.

$$\mathbf{K}^e = \int_{\Omega_e} \mathbf{B}^{eT} \mathbf{D}^e(\mathbf{x}) \mathbf{B}^e d\Omega_e \quad (2)$$

where \mathbf{u}^e = nodal displacement vector; \mathbf{F}^e = load vector; \mathbf{B}^e = strain-displacement matrix which contains gradients of the interpolating functions; $\mathbf{D}^e(\mathbf{x})$ = constitutive matrix (variable); and Ω_e is the domain of element e . In the present work, the elasticity matrix $\mathbf{D}^e(\mathbf{x}) = \mathbf{D}^e(x,y)$ is assumed to be a function of spatial coordinates.

The integral in Eq. (2) is evaluated by Gauss quadrature, and the matrix $\mathbf{D}^e(\mathbf{x})$ is specified at each Gaussian integration point. Thus for two-dimensional problems, the resulting integral becomes

$$\mathbf{K}^e = \sum_{i=1}^N \sum_{j=1}^N \mathbf{B}_{ij}^{eT} \mathbf{D}_{ij}^e \mathbf{B}_{ij}^e J_{ij} w_i w_j \quad (3)$$

where the subscripts i and j refer to the Gaussian integration points, J_{ij} is the determinant of the Jacobian matrix, and w_i are the Gaussian weights.

A comparison between homogeneous and graded elements by means of a simple element using spectral analysis reveals further differences between elements. Consider a square element of unit length with the origin at the left bottom corner. The Young's modulus is given by

$$E(x) = E_1 e^{\beta x} \quad (4)$$

where $E_1 = 1.0$ and $\beta = 0.0$ for the homogeneous material case and $\beta = 1.0$ for the nonhomogeneous material case. Figs. 3 and 4 illustrate a comparison between the two cases for the Q4 element. The following observations can be made.

- As expected, the number of rigid modes (3) and spurious deformation (zero energy) modes (e.g., two spurious modes for Q4 with 1×1 Gauss integration) is the same for both cases (homogeneous and graded elements).
- Symmetry, as expressed by the deformation modes (eigenvectors) is broken for graded elements, i.e., there are no repeated eigenvalues.
- The total energy ($U_i = \lambda_i / 2, i = 1, \dots$ NDOFs) increases for the FGM with $\beta > 0$. Here NDOFs indicates the number of degrees of freedom in the element and λ_i indicates the i th eigenvalue.

Verification of UMAT

Analytical solutions (Erdogan and Wu 1997) for isotropic FGMs where material properties vary exponentially along the x direction are used as a reference to verify the implementation of the *UMAT*.

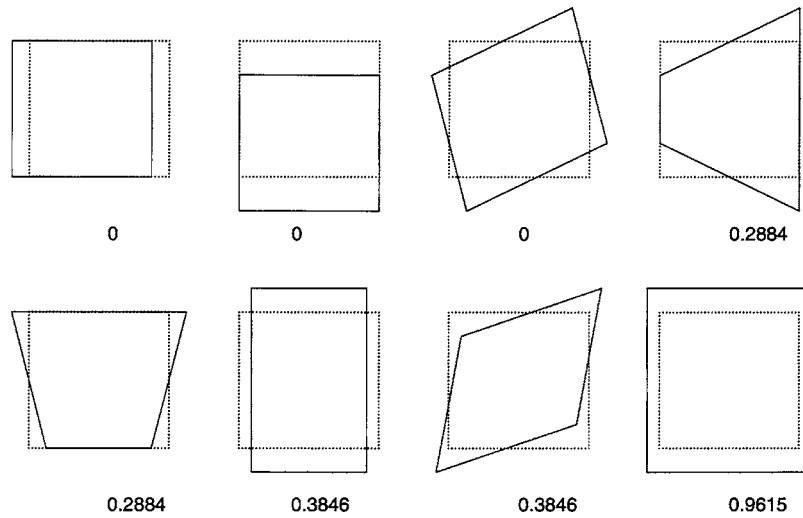


Fig. 3. Eigenanalysis for Q4 (2×2 Gauss quadrature) and $\beta=0$ (homogeneous material). The numbers indicate the eigenvalues (λ_i).

Moreover, by means of this example, the benefit of using the graded element approach is illustrated by comparing unaveraged nodal stresses obtained with graded elements with those obtained from the layered approach.

Consider a rectangular finite plate of width $W=9$ and height $H=9$ as illustrated in Fig. 5. A constant traction of $\sigma_t=1$ perpendicular to the material gradation is applied to the top edge and displacement boundary conditions, $u_2=0$ for the bottom edge and $u_1=0$ for the left bottom node, are prescribed [see Fig. 5(b)]. Consistent units are employed. The finite element mesh consists of 81 Q8 elements, which are either graded or homogeneous elements. The elastic modulus varies exponentially along the x direction

$$E(x) = E(0)e^{\beta x}, \quad \beta = \frac{1}{W} \log\left(\frac{E(W)}{E(0)}\right) \quad (5)$$

where $E(0)=1$, $E(W)=8$, and β is an independent material non-homogeneity parameter which has units $[\text{length}]^{-1}$. Therefore $1/\beta$

is the length scale of nonhomogeneity. A constant Poisson's ratio of 0.3 is employed. Plane stress condition and 3×3 Gauss quadrature are adopted.

For tension loading, the compatibility condition $\partial \varepsilon_{yy}^2 / \partial x^2 = 0$, yields strain and stress fields given by (Erdogan and Wu 1997)

$$\varepsilon_{yy} = Ax + B, \quad (6)$$

$$\sigma_{yy}(x) = E'(0)e^{\beta x}(Ax + B) \quad (7)$$

where $E'(0)$ is $E(0)$ for plane stress and $E(0)/(1-\nu^2)$ for plane strain. The coefficients A and B are determined from the following equilibrium conditions for the tension loading:

$$\int_0^W \sigma_{yy}(x) dx = N \quad \text{and} \quad \int_0^W \sigma_{yy}(x)x dx = M \quad (8)$$

where N is $\sigma_t W$ and M is assumed to be zero. So the stress distribution is (Erdogan and Wu 1997)

$$\sigma_{yy}(x) = \frac{\beta N}{2} e^{\beta x} \left[\left(\frac{W\beta^2 e^{\beta W} - 2\beta e^{\beta W} + W\beta^2 + 2\beta}{e^{\beta W}\beta^2 W^2 - e^{2\beta W} + 2e^{\beta W} - 1} \right) x + \frac{e^{\beta W}[e^{\beta W}(-W^2\beta^2 + 3\beta W - 4) + W^2\beta^2 - 2\beta W + 8] - \beta W - 4}{(e^{\beta W} - 1)(e^{\beta W}\beta^2 W^2 - e^{2\beta W} + 2e^{\beta W} - 1)} \right] \quad (9)$$

Fig. 6 compares unaveraged nodal stresses interpolated from stresses at Gauss points using graded and homogeneous Q8 elements. The abscissa indicates the horizontal distance from the zero coordinate. The ordinate indicates σ_y . Bending effects due to both the exponential material gradation and the constant traction perpendicular to the material gradation lead to the trend that the exact solution first increases and then decreases with the increase of x (see Fig. 6). The homogeneous Q8 elements show piecewise variation due to the stepwise approximation of the continuous material property. However, the graded Q8 elements show remarkably smooth stress variation and match with the analytical solution quite well demonstrating the verification of the *UMAT* implementation. The relatively small differences observed between the analytical solutions and the numerical results using

the graded Q8 elements may be attributed to the fact that the analytical solution is derived based on an infinite plate length, while the numerical results are determined based on a finite length. Regarding performance of both graded and homogeneous elements, the graded elements are superior to homogeneous elements for the following reasons: (1) unaveraged stresses using layered elements show large differences between the boundary where material property is not continuous, while graded elements predict almost identical unaveraged stresses at the same boundary; (2) unaveraged stresses using graded elements show much better approximation to the exact solution in every element than those using homogeneous elements. Nodal averaging schemes and refined meshes can improve the performance of the layered approach. However, averaging of nodal stresses may lead to

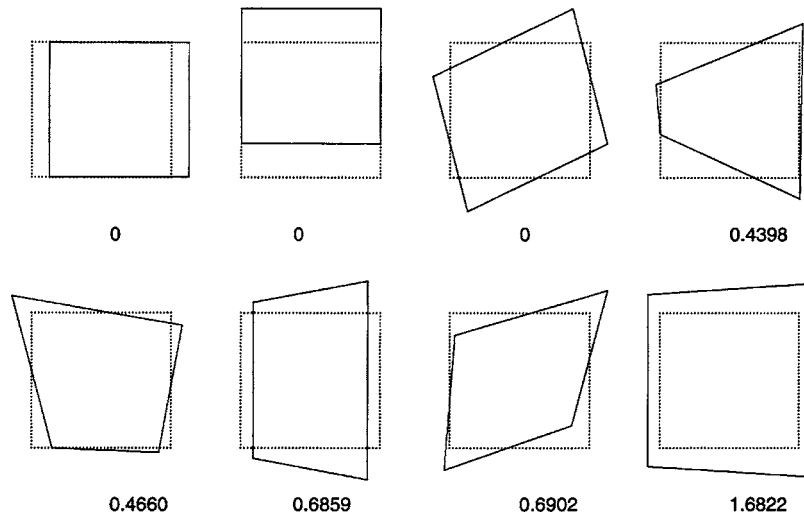


Fig. 4. Eigenanalysis for Q4 (2×2 Gauss quadrature) and $\beta=1$ (FGM). The numbers indicate the eigenvalues (λ_i).

inaccurate responses especially in the vicinity of corners, cracks or other discontinuities. Furthermore, refined meshes can increase computational expense, particularly for three dimensional analysis which is generally required in pavement analysis due to geometric asymmetries. Notice that the use of graded elements leads to averaging or approximation process in the material properties [by adopting a variable D matrix—see Eq. (2)] rather than averaging at the end, i.e., after discretization and solution of the boundary value problem.

Application of UMAT for a Pavement System

A numerical example was chosen to coincide with a pavement case study previously conducted at the University of Illinois involving highway I-155, a four-lane divided interstate pavement in central Illinois near the town of Lincoln (see Fig. 7). This pavement section has received considerable attention because it has shown several surface related problems, such as block cracking, thermal cracking, and longitudinal surface cracking (Lippert 1993; Huber and Scherocman 1994). I-155 is a full-depth asphalt pavement, with 375 mm of hot-mix asphalt on a lime-stabilized clay subgrade.

Although a detailed case study of I-155 is beyond the scope of this paper, it is hoped that the theoretical framework and preliminary analysis conducted herein will be of future benefit for forensic investigations of I-155 and other pavements showing

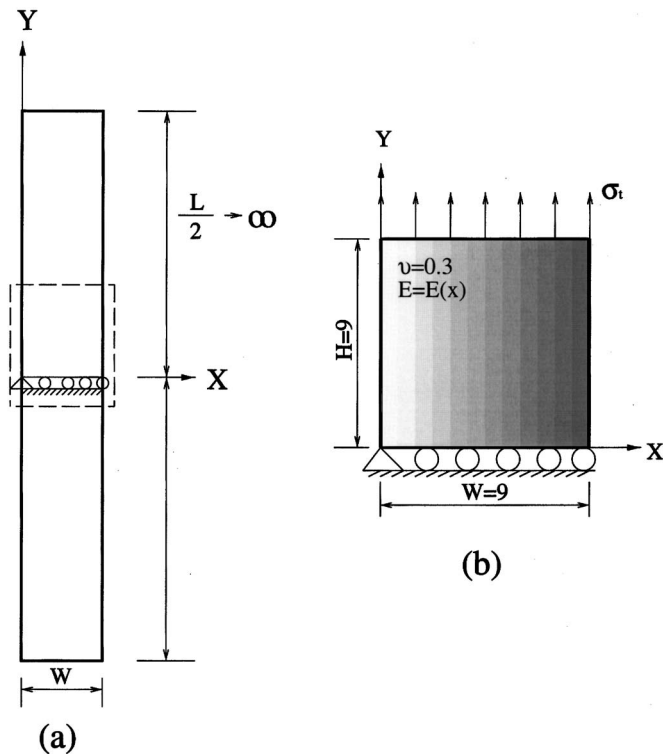


Fig. 5. Functionally graded plate: (a) geometry—the domain covered by dotted line indicates the geometry used in the FEA; (b) a finite plate used in FEA with boundary conditions and material properties

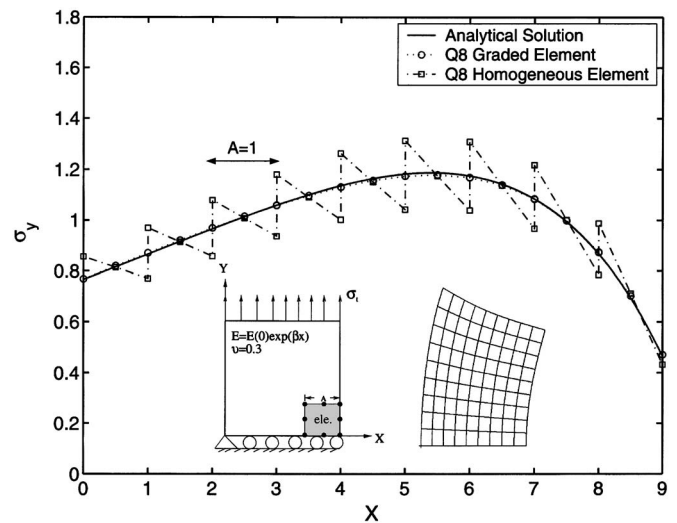


Fig. 6. Stress distribution (σ_y) using Q8 elements for tension loading perpendicular to the exponential material gradation along the x direction. The inserts show the specimen before and after deformation.

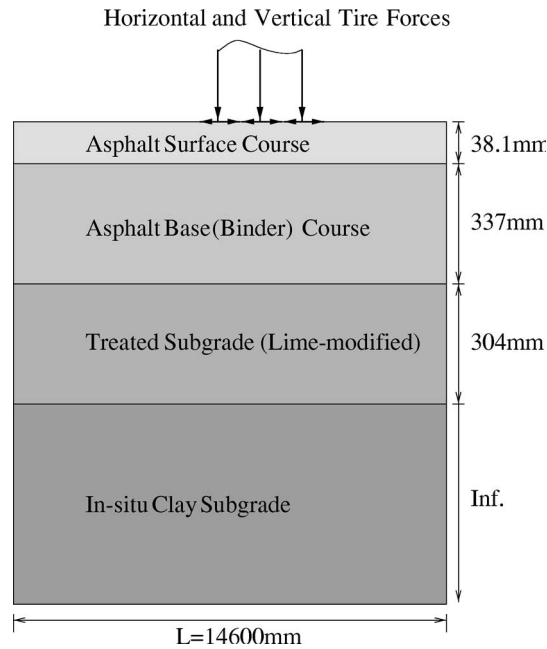


Fig. 7. Typical pavement cross section for Illinois I-155

premature distress development. Early testing of recovered binder from I-155 indicated very severe aging of the surface. For example, the binder viscosity at 60°C which was approximately 4,000 Poise just after construction, had increased to over 100,000 Poise near the surface after three years in service.

Input Parameters and Assumptions

To evaluate the response of the I-155 pavement structure using the graded finite element approach, a description of the asphalt mixture property gradients as a function of depth was needed, particularly near the pavement surface where gradients are most severe. Gradients in material properties within a given pavement asphalt arise for two main effects: (1) oxidative hardening (aging) of the asphalt layer, particularly near the surface and (2) temperature gradients within the pavement, giving rise to material gradients due to the extreme sensitivity of asphalt modulus and Poisson's ratio to temperature. Unfortunately, insufficient mixture testing of materials obtained at multiple depth in the pavement was available at the time of this study to completely describe the material property gradients on I-155. Fortunately, empirical models have been developed by Mirza and Witczak (1995) and Witczak (1998). Thus, they were used to approximate the concrete material property gradients based upon asphalt viscosity, pavement age, depth below the pavement surface, air void content, asphalt content, etc. The severe aging gradients obtained with these models were found to be consistent with those reported in the experimental field investigations of Huber and Scherocman (1994) and Lippert (1993). Table 1 summarizes the inputs used in the global aging model and modulus prediction model.

In order to obtain pavement moduli under a realistic temperature gradient, it was necessary to predict pavement temperatures versus depth at I-155. To accomplish this, the enhanced integrated climatic model (EICM) (Larson and Dempsey 1997) was employed along with measured air temperature at Lincoln, Illinois as tracked by the Illinois State Water Survey at the University of Illinois at Urbana-Champaign. The EICM program is a one-dimensional coupled heat and moisture flow model, which was used in the current study to predict pavement temperature profiles

Table 1. Input Parameters for Global Aging Model Runs to Compute Asphalt Concrete Modulus Gradient with Depth (T Denotes Temperature)

Input Parameter	Value
Cumulative percent retained on 3/4" sieve	0
Cumulative percent retained on 3/8" sieve	8.0
Cumulative percent retained on 4 Sieve	42.0
Percent passing 200 sieve	4.6
Volume of effective asphalt content	10.0
Loading time (s)	0.1
Mean average air temperature	51.4
Pavement age in months	96
In-place air voids (percent)	7
$A = (\log \text{Penetration at } T_1 - \log \text{Penetration at } T_2) / (T_1 - T_2)$	11.0248
$VTS = (\log \log \text{viscosity at } T_2 - \log \log \text{viscosity at } T_1) / (\log T_1 - \log T_2)$	-3.7053

as a function of measured air temperature, latitude, percent sunshine, emissivity, surface short wave absorptivity, maximum convection coefficient, wind speed, and several other factors. The predicted pavement temperature versus depth for I-155, at 5 a.m. on July 4, 1997 is given in Fig. 8. Although the selection process of this specific temperature event was somewhat arbitrary for the purposes of this analysis, the selected temperature profile appeared to create a fairly high stiffness gradient (which was desirable from the standpoint of illustrating differences between the graded element approach and the layered approach). Temperature profiles from cooler months were found to produce higher overall pavement stiffness, but much lower stiffness gradients. This is because the mixture stiffness, as obtained from Witczak (1998) modulus prediction model, tends to approach a plateau at approximately 21 GPa. Since all other model coefficients were held constant, this mixture plateau is caused primarily by a plateau in the binder stiffness master curve as the glassy modulus is approached. In the case of an aged pavement such as I-155, a very low stiffness gradient was predicted during the winter months and even portions of the spring months.

Figs. 9 and 10 present the dynamic modulus and Poisson's ratio versus depth based upon the empirical prediction models of Mirza

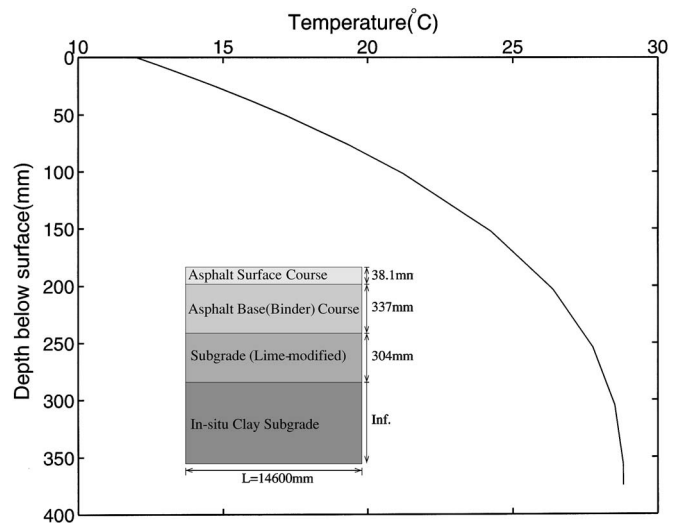


Fig. 8. Predicted pavement temperature versus depth for I-155, near Lincoln, Illinois, at 5 a.m. on July 4, 1997

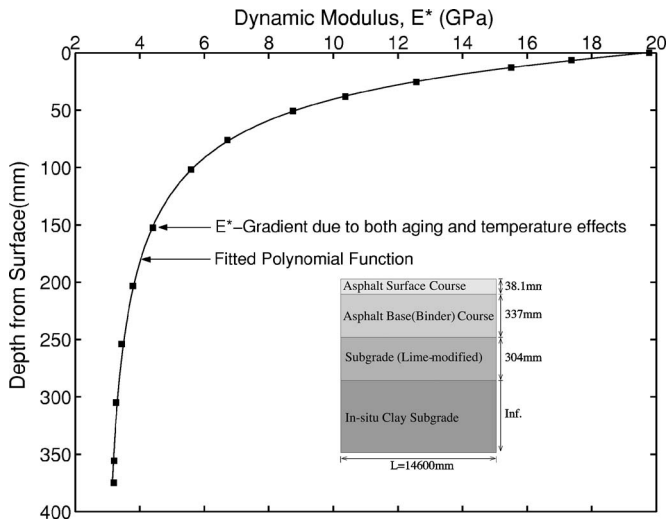


Fig. 9. Dynamic modulus versus depth computed from aging, climatic, and modulus models with fitted function

and Witczak (1995). Clearly, the combination of temperature and aging gradients creates a large gradient of predicted E^* with depth for the selected conditions, particularly in the first 100 mm of depth. Poisson's ratio is predicted to increase with depth in pavement. Simple polynomial models were fit, as shown on Figs. 9 and 10, to facilitate input of these parameters into the graded and layered finite element FE models.

Pavement Model

A four-lane pavement structure of length $2L=14,600$ mm with thickness of surface and binder 374.7 mm, thickness of subgrade 304.1 mm, and thickness of soil 9144 mm was analyzed in conjunction with the *UMAT* where graded and homogeneous elements were implemented. To reduce the model size, a symmetry condition was adopted. Displacement boundary conditions of $u_2=0$ for the bottom edge were prescribed. Normal and shear stresses induced by a truck tire, based upon measured contact stresses by Myers et al. (1999) for a radial tire, were used. For

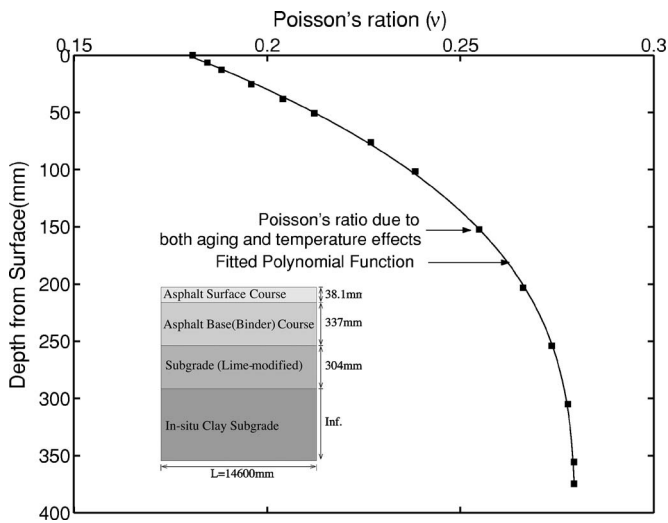


Fig. 10. Poisson's ratio versus depth computed from aging, climatic, and modulus models with fitted function

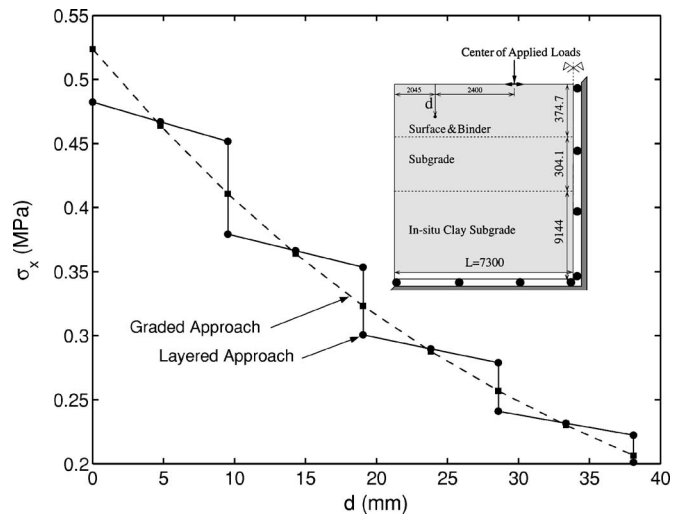


Fig. 11. Graded model versus layered model: Unaveraged horizontal stress (σ_x) with depth (d) at the location where maximum tensile stresses occur

simplicity, a single radial truck tire was applied to the pavement surface because the purpose of this analysis is primarily focused on making a relative comparison between the graded element and layered element approaches. The material properties where aging and temperature are taken into account were applied to surface and binder courses (see Figs. 9 and 10). Young's modulus was taken as $E=138$ MPa in the lime-cemented subgrade and $E=35$ MPa in the soil. Four layered pavement systems were constructed using 23,840 Q8 elements. The plane strain condition was adopted with 3×3 Gauss quadrature.

Pavement Modeling Results

Three strategic evaluation regions within the pavement model were examined to quantify the difference between graded elements and the traditional layered approach as shown in Figs. 11–14. Fig. 11 illustrates unaveraged horizontal stress profiles for graded and homogeneous elements along the depth at the

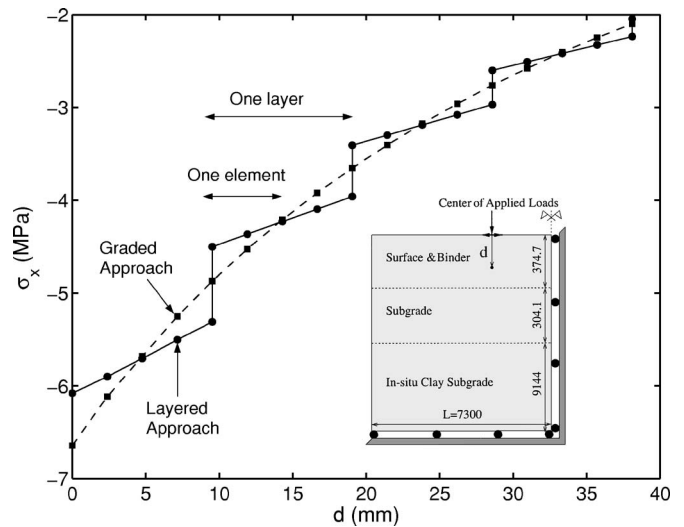


Fig. 12. Graded model versus layered model: Unaveraged horizontal stress (σ_x) with depth (d) along the center of the tire loads

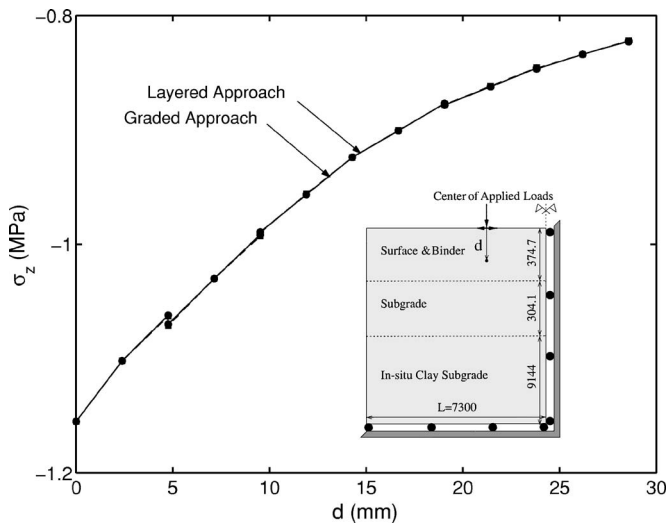


Fig. 13. Graded model versus layered model: Unaveraged vertical stress (σ_z) with depth (d) along the center of the tire loads

location where maximum surface tension occurs. It is located at 2,400 mm away from the center of the applied load. The abscissa indicates the vertical evaluation depth to 40 mm below the surface and the ordinate indicates unaveraged horizontal stresses, i.e., σ_x . Along the boundaries where material properties are not continuous, layered elements predict a large difference in unaveraged stress, while graded elements predict almost identical unaveraged stresses, illustrating the superiority of graded elements. Moreover, surface tensile stresses, which are important in thermal cracking problems, are underestimated when homogeneous elements are used, as shown in Fig. 11.

Fig. 12 shows the unaveraged tensile stresses using graded and homogeneous elements. The abscissa indicates the vertical evaluation depth up to 40 mm below the surface, starting just below the center of the applied loads. The ordinate indicates the horizontal stress, i.e., σ_x . As expected, homogeneous Q8 elements show piecewise variation. However, this does not occur with the graded elements. Moreover, the surface stresses are underestimated when homogeneous elements are adopted. A benefit of graded elements is pronounced when the stiffness gradient is severe (see Fig. 9) for this problem. Notice that although the realistic tire loads (Myers et al. 1999) consisting of the normal and shear traction are applied, surface tension under the tire loads are not observed in this simulation.

Unaveraged σ_z versus vertical depth is plotted for two different approaches in Fig. 13. The absolute magnitude of σ_z decreases as the vertical distance increases. However, for σ_z , which is an important stress component in evaluating rutting potential in pavements, the two approaches yield almost identical results. Unaveraged tensile strains for graded and layered approaches are illustrated in Fig. 14. The abscissa indicates the vertical distance from the bottom of the surface to 85 mm above this point, directly beneath the center of the applied loads. The absolute magnitude of ϵ_x decreases almost linearly with position. As expected, the difference between graded and layered approaches are insignificant in this case, where material gradations are small. Thus, for the purpose of a traditional fatigue analysis (bottom-up cracking due to bending induced tensile stresses), the traditional layered approach may suffice.

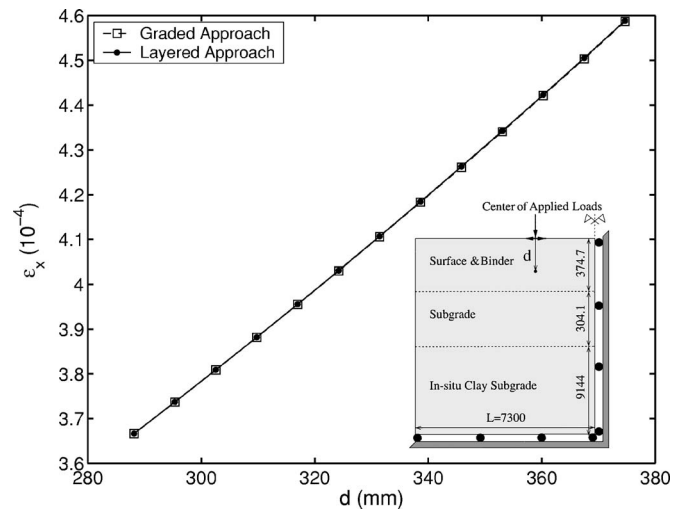


Fig. 14. Graded model versus layered model: Unaveraged horizontal strain (ϵ_x) with depth (d) along the center of the tire loads

Summary and Conclusion

This paper presents the development and application of graded finite elements for pavement analysis. A theoretical formulation for the graded finite element method was provided. The implementation of the *UMAT* was verified by comparing the numerical results with the analytical solutions by means of the isotropic graded materials where Young's modulus varies perpendicular to the loading direction. Numerical examples illustrate the benefits of using graded elements.

The combination of temperature and aging gradients led to the prediction of a large E^* gradient with depth for the selected conditions on interstate pavement I-155 in Illinois. The stiffness gradient was found to be severe as far down as 100 mm of depth.

In general, the graded finite element method used here provides superior results over the conventional finite element solution, which involves assigning mixture properties in layers. As expected, the differences were most pronounced when evaluating near-surface pavement responses, where severe material gradients are present due to environmental exposure. The use of fine meshes and stress averaging techniques can be used to minimize errors in the layered approach. However, both of these techniques can have significant drawbacks. For instance, very fine meshes are computationally expensive, particularly when conducting three-dimensional analyses. Furthermore, averaging of nodal stresses was shown to lead to inaccuracies at layer interfaces of different materials, and may lead to inaccuracies in areas of high stress gradients, such as in the vicinity of cracks or other discontinuities.

Acknowledgments

We are grateful to the support from the SemMaterials (previously Koch Materials) Company and the National Science Foundation (NSF) through the GOALI Project No. CMS 0219566 (Program Manager, P. N. Balaguru). We also thank three anonymous reviewers for their insightful remarks which contributed to improve the manuscript. Any opinions expressed herein are those of the writers and do not necessarily reflect the views of the sponsors.

Appendix

The *ABAQUS* user subroutine *UMAT* for graded elements is presented here. It is written in Fortran language.

```
c
c -----
c      * REFERENCE
c      W.G. Buttlar, G.H. Paulino and S.H. Song
c      (University of Illinois at Urbana-Champaign)
c      "Application of graded finite elements for asphalt paving"
c      submitted to ASCE Journal of Engineering Mechanics
c
c      * PROBLEM DESCRIPTION
c      This UMAT user subroutine is for isotropic and isothermal materials.
c      This subroutine handles for 3-D and plane strain problems.
c      This subroutine needs to be modified for plane stress.
c      Both homogeneous and graded properties are possible by selecting
c      appropriate functional form of "props".
c      This UMAT is based on "direct integration method".
c
c      * IMPORTANT NOTICE
c      For new problems, choose the function for
c      the material variation and the values of "props".
c      After that, go to the section -CHANGE- and change the function and
c      values accordingly.
c -----
c
c      subroutine UMAT(stress, statev, ddsdde, sse, spd, scd,
c      & rpl, ddsddt, drplde, drpldt,
c      & stran, dstran, time, dtime, temp, dtemp, predef, dpred, cmname,
c      & ndi, nshr, ntens, nstatv, props, nprops, coords, drot, pnwtdt,
c      & celent, dfgrd0, dfgrd1, noel, npt, layer, kspt, kstep, kinc)
c
c      include 'ABA_PARAM.INC'
c
c      character*80 cmname
c      dimension stress(ntens), statev(nstatv),
c      & ddsdde(ntens, ntens),
c      & ddsddt(ntens), drplde(ntens),
c      & stran(ntens), dstran(ntens), time(2), predef(1), dpred(1),
c      & props(nprops), coords(3), drot(3,3), dfgrd0(3,3), dfgrd1(3,3)
c
c      Determine material properties based on global coordinates of gauss points.
c
c      coords(1) is X-coordinate of gauss points.
c      coords(2) is Y-coordinate of gauss points.
c      coords(3) is Z-coordinate of gauss points.
c      props is defined by users.
c      The function can be also defined by users.
c
c      ---CHANGE-----
c      E=props(1)+props(2)*coords(1)+props(3)*coords(2)
c      & +props(4)*coords(3)
c      v=props(5)+props(6)*coords(1)+props(7)*coords(2)
c      & +props(8)*coords(3)
c -----
c
c      Determine Lamé's constants
c
c      amu is mu
```

```

c      alambda is lambda
c
c      amu=E/2.0d0/(1.0d0+v)
c      alambda=E*v/(1.0d0+v)/(1.0d0-2.0d0*v)
c
c      Determine the tangent(Jacobian) matrix
c
c      ndi is number of normal stresses (e.g. Sxx, Syy, Szz)
c      nshr is number of shear stresses (e.g. Sxy)
c      ntens is dimension of constitutive matrix(ntens=ndi+nshr)
c
c      do i=1, ndi
c          do j=1, ndi
c              if (i.eq.j) then
c                  ddsdde(i,i)=alambda+2.0d0*amu
c              else
c                  ddsdde(i,j)=alambda
c              endif
c          enddo
c      enddo
c      do i=ndi+1, ntens
c          ddsdde(i,i)=amu
c      enddo
c
c      Determine the stress and update the stress
c
c      do i=1, ntens
c          do j=1, ntens
c              stress(i)=stress(i)+ddsdde(i,j)*dstran(j)
c          enddo
c      enddo
c
c      return
c      end

```

References

- AASHTO. (2002). *Development of 2002 design guide using mechanistic principles to improve pavement design*, Washington D.C.
- ABAQUS. (2004). *User manual version 6.2*. H.K.S. Inc., Pawtucket, R.I.
- Bozkurt, D., and Buttlar, W. G. (2002). "Three-dimensional finite element modeling to evaluate benefits of interlayer stress absorbing composite for reflective cracking mitigation." *Proc., Federal Aviation Administration Airport Technology Transfer Conference*, Washington, D.C.
- Erdogan, F., and Wu, B. H. (1997). "The surface crack problem for a plate with functionally graded properties." *J. Appl. Mech.*, 64(3), 449–456.
- Hirano, T., Teraki, J., and Yamada, T. (1990). "On the design of functionally gradient materials." *Proc., First Int. Symposium on Functionally Gradient Materials*, M. Yamanouchi, M. Koizumi, T. Harai, and I. Shiota, eds., Functionally Gradient Materials Forum, October 8–9, 5–10.
- Huber, G., and Scherocman, J. A. (1994). "Investigations of premature distress: Highway US 36 and Interstate Highway 155." *Final Project Rep.*, Illinois Department of Transportation, Springfield, Ill.
- Hughes, T. J. R. (1987). *The finite element method: Linear static and dynamic finite element analysis*, Prentice-Hall, Englewood Cliffs, N.J.
- Igari, T., Notomi, A., Tsunoda, H., Hida, K., Koto, T., and Kunishima, S. (1990). "Material properties of functionally gradient material for fast breed reactor." *Proc., First Int. Symposium on Functionally Gradient Materials*, M. Yamanouchi, M. Koizumi, T. Hirai, and I. Shiota, eds., Functionally Gradient Materials Forum, October 8–9, 209–214.
- Kim, J. (1999). "Three-dimensional finite element modeling of multi-layered system." PhD dissertation, University of Illinois at Urbana-Champaign.
- Kim, J., and Buttlar, W. G. (2002). "Analysis of reflective crack control system involving reinforcing grid over base-isolating interlayer mixture." *J. Transp. Eng.*, 128(4), 375–384.
- Kim, J.-H., and Paulino, G. H. (2002a). "Isoparametric graded finite element for nonhomogeneous isotropic and orthotropic materials." *J. Appl. Mech.*, 69(4), 502–514.
- Kim, J.-H., and Paulino, G. H. (2002b). "Finite element evaluation of mixed-mode stress intensity factors in functionally graded materials." *Int. J. Numer. Methods Eng.*, 53(8), 1903–1935.
- Kim, J.-H., and Paulino, G. H. (2003). "T-stress, mixed mode stress intensity factors, and crack initiation angles in functionally graded materials: A unified approach using the interaction integral method." *Comput. Methods Appl. Mech. Eng.*, 192(11/12), 1463–1494.
- Larson, G., and Dempsey, B. J. (1997). "Enhanced integrated climatic model, version 2.0." *Rep. No. DTFA MN/DOT 72114*, Minnesota Road Research Program, Minnesota Dept. of Transportation, Maplewood, Minn.
- Lippert, D. L. (1993). "A review of cracking on full-depth bituminous pavement (longitudinal cracking)." *Internal Rep.*, Illinois Department of Transportation, Springfield, Ill.
- Mirza, M. W., and Witczak, M. W. (1995). "Development of a global aging system for short and long term aging of asphalt cements." *J. Assoc. Asph. Paving Technol.*, 64, 393–430.

- Myers, L. A., Roque, R., and Birgisson, B. (2001). "Use of two-dimensional finite element analysis to represent bending response of asphalt pavement structures." *Int. J. Pavement Eng.*, 2, 201–214.
- Myers, L. A., Roque, R., Birgisson, B., and Drakos, C. (1999). "Measurement of contact stresses for different truck tire types to evaluate their influence on near-surface cracking and rutting." *Transportation Research Board* (CD-Rom), Washington D.C.
- Oonishi, H., Noda, T., Ito, S., Kohda, A., Yamamoto, H., and Tsuji, E. (1994). "Effect of hydroxyapatite coating on bone growth into porous Titanium alloy implants under loaded conditions." *J. Appl. Biomater.*, 5(1), 23–27.
- Sangpetngam, B., Birgisson, B., and Roque, R. (2004). "A multi-layer boundary element method for the evaluation of top-down cracking in hot mix asphalt pavements." *Transportation Research Board* (CD-Rom), Washington D.C.
- Santare, M. H., and Lambros, J. (2000). "Use of graded finite elements to model the behavior of nonhomogeneous materials." *J. Appl. Mech.*, 67(4), 819–822.
- Tani, J., and Liu, GR. (1993). "Surface waves in functionally gradient piezoelectric plates." *JSME Int. J., Ser. A*, 36(2), 152–155.
- Watari, F., Yokoyama, A., Saso, F., Uo, M., Ohkawa, S., and Kawasaki, T. (1996). "EPMA elemental mapping of functionally graded dental implant in biocompatibility test." *Proc., Fourth Int. Symposium on Functionally Graded Materials*, I. Shiota and Y. Miyamoto, eds., Elsevier, October 21–24, 749–754.
- Witczak, M. W. (1998). "Development of relationships between binder viscosity and stiffness." *SUPERPAVE Support and Performance Models Contract, FHWA No. DTFH 61-94-R-00045, Team Technical Rep.*, University of Maryland, College Park, Md.